Adiabatic Effectiveness Measurements of Endwall Film-Cooling for a First-Stage Vane

D. G. Knost

K. A. Thole

Mechanical Engineering Department,
Virginia Polytechnic Institute and State University,
Blacksburg, VA 24061

In gas turbine development, the direction has been toward higher turbine inlet temperatures to increase the work output and thermal efficiency. This extreme environment can significantly impact component life. One means of preventing component burnout in the turbine is to effectively use film-cooling whereby coolant is extracted from the compressor and injected through component surfaces. One such surface is the endwall of the first-stage nozzle guide vane. This paper presents measurements of two endwall film-cooling hole patterns combined with cooling from a flush slot that simulates leakage flow between the combustor and turbine sections. Adiabatic effectiveness measurements showed the slot flow adequately cooled portions of the endwall. Measurements also showed two very difficult regions to cool, including the leading edge and pressure side-endwall junction. As the momentum flux ratios were increased for the film-cooling jets in the stagnation region, the coolant was shown to impact the vane and wash down onto the endwall surface. Along the pressure side of the vane in the upstream portion of the passage, the jets were shown to separate from the surface rather than penetrate to the pressure surface. In the downstream portion of the passage, the jets along the pressure side of the vane were shown to impact the vane thereby eliminating any uncooled regions at the junction. The measurements were also combined with computations to show the importance of considering the trajectory of the flow in the near-wall region, which can be highly influenced by slot leakage flows. [DOI: 10.1115/1.1811099]

Introduction

Combustion turbine engines have become an integral part of our daily lives through propelling aircraft, tanks, and large naval ships and providing peaking power on the electrical grid. The technology of the turbine engine needs to continue to grow to provide more power at a higher efficiency in today's more environmentally conscious, yet energy-thirsty, world. The power output and efficiency of a turbine engine depend on the fluid temperature entering the turbine, with engine development moving toward increasing turbine temperatures.

As turbine inlet temperatures continue to rise the metallurgical limits of the machine have been pushed and frequently exceeded. One method of combating the overheating problem is the use of film-cooling holes whereby cooler air is extracted from the compressor, bypasses the combustor, and is injected through discrete holes in the vane and endwall surfaces. Film-cooling hole placement, particularly in the endwall region, has traditionally been based on designer experience. In addition to film cooling, most turbines have a slot at the combustor-turbine interface where cooler gases leak through. If designed properly, this leakage flow could be relied on as a source of coolant. It is also important to recognize the importance of overall aerodynamic penalties for endwall cooling.

The goal of this research was twofold. The first goal was to compare two different film-cooling hole patterns, which were based on different design philosophies. The second goal was to determine how the leakage slot flow at the combustor-turbine interface could be used to cool the turbine platform and also how this slot flow might affect the downstream film cooling. One region in particular that was assessed from a cooling standpoint was the leading-edge region of the vane whereby a range of coolant injection levels were evaluated.

Contributed by the International Gas Turbine Institute (IGTI) of THE AMERICAN SOCIETY OF MECHANICAL ENGINEERS for publication in the ASME JOURNAL OF TURBOMACHINERY. Paper presented at the International Gas Turbine and Aeroengine Congress and Exhibition, Vienna, Austria, June 13–17, 2004, Paper No. 2004-GT-53326. Manuscript received by IGTI, October 1, 2003; final revision, March 1, 2004. IGTI Review Chair: A. J. Strazisar.

Summary of Past Literature

There have been a number of studies documenting endwall film cooling and a number of studies documenting cooling from the leakage gap at the turbine-combustor junction. As will also be discussed in this summary, there has been only one study presented in the literature that has combined endwall film cooling with coolant leakage from an upstream slot.

Detailed endwall film-cooling results have been conducted by Friedrichs et al. [1–3]. The results of their first study [1], which were all surface measurements or visualization, indicated a strong influence of the secondary flows on the film cooling and an influence of the film cooling on the secondary flows. Their data showed that the angle at which the coolant leaves the hole did not dictate the coolant trajectory, except near the hole exit. Furthermore, the endwall cross flow was altered so that it was turned toward the inviscid streamlines, which was due to the film-cooling injection.

There have been a few studies that have measured endwall heat transfer as a result of injection from a two-dimensional (2D) flush slot just upstream of the vane. Blair [4] measured adiabatic effectiveness levels and heat transfer coefficients for a range of blowing ratios through a flush slot placed just upstream of the leading edges of his single-passage channel. One of the key findings was that the endwall adiabatic effectiveness distributions showed extreme variations across the vane gap with much of the coolant being swept across the endwall toward the suction-side corner. Granser and Schulenberg [5] reported similar adiabatic effectiveness results in that higher values occurred near the suction side of the vane. Based on their measurements, Roy et al. [6], however,

indicated that the coolant migrated toward the pressure side of the vane. Their measurements indicated reduced values of local heat transfer coefficients at the leading edge when slot cooling was present relative to no slot cooling.

A series of experiments have been reported for various injection schemes upstream of a nozzle guide vane with a contoured endwall by Burd and Simon [7], Burd et al. [8], and Oke et al. [9,10]. In these studies [7–9], coolant was injected from an interrupted flush slot that was inclined at 45 deg just upstream of their vane. Similar to others, they found that most of the slot coolant was directed toward the suction side at low-slot flow conditions. As they increased the percentage of slot flow to 3.2% of the exit flow, their measurements indicated better coverage occurred between the airfoils.

Colban et al. [11,12] reported flow-field and endwall effectiveness contours for a backward-facing slot with several different coolant exit conditions. Their results indicated the presence of a tertiary vortex that developed in the vane passage due to a peaked total pressure profile in the near-wall region. For all of the conditions simulated, the effectiveness contours indicated the coolant from the slot was swept toward the suction surface. While this study was completed for the same vane geometry as that reported in this paper, the slot geometry has been altered to be flush with the endwall surface.

Zhang and Moon [13] tested a two row film-cooling configuration upstream of a contoured endwall. Upstream of these two rows of film-cooling holes was placed either a flush wall or a backward facing step. In making direct comparisons between these two configurations, measured effectiveness levels were reduced considerably in the case of the backward-facing step configuration. They attributed these reduced effectiveness levels to the increased secondary flows that were present.

The only two studies to have combined an upstream slot with film-cooling holes in the passage of the vane were those of Kost and Nicklas [14] and Nicklas [15] and a CFD study previously reported by Knost and Thole [16] as those on this paper. One of the most interesting results from the Kost and Nicklas [14] and Nicklas [15] studies was that they found for the slot flow alone, which was 1.3% of the passage mass flow, the horseshoe vortex became more intense. This increase in intensity resulted in the slot coolant being moved off of the endwall surface and heat transfer coefficients that were over three times that measured for no-slot flow injection. They attributed the strengthening of the horseshoe vortex to the fact that for the no-slot injection, the boundary layer was already separated with fluid being turned away from the endwall at the injection location. Given that the slot had a normal component of velocity, injection at this location promoted the separation and enhanced the vortex. Their adiabatic effectiveness measurements indicated higher values near the suction side of the vane due to the slot-coolant migration.

The CFD study results presented by Knost and Thole [16], for the same geometry and coolant flow conditions as presented in this paper, indicated the presence of a warm ring on the endwall around the vane where no coolant was present despite the combined slot cooling and film cooling. Based on this computational study and lack of experimental data in the literature for a realistic hole pattern combined with an upstream slot representing the combustor-turbine interface, there was a need to verify the cooling problems associated with the endwall of a turbine platform.

Design of Endwall Cooling Schemes

Two realistic cooling hole patterns for the platform of the vane were developed based on industry input, as shown in Fig. 1. Also shown in this figure are iso-velocity contours, hole injection directions, and for pattern 2, the location of a gutter. A gutter, which is the joint between the two mating platforms, has the potential of having coolant leakage, but was not simulated in our studies. The airfoil geometry used in the current study is a commercial first-stage vane previously described by Radomsky and Thole [17]. The vane is two-dimensional with the midspan modeled along the entire span.

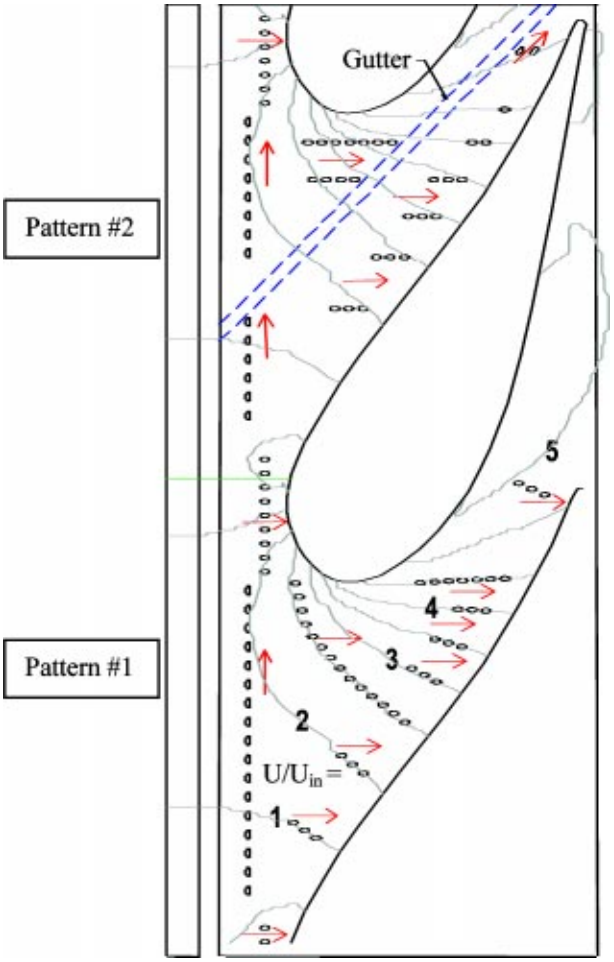

Fig. 1 The two film-cooling patterns that were simulated in this study with iso–velocity contours (U/U_{inlet}) and injection direction for the cooling holes

Table 1 provides a summary of parameters relevant to both cooling-scheme designs. Both cooling hole patterns included a two-dimensional flush slot located $0.31C_a$ upstream of the vane stagnation, representing the combustor-turbine interface. The slot injected at an angle of 45 deg with respect to the endwall and had a slot length (flow-path length) to width (cross-sectional width) of 1.8.

Downstream of the slot, two different endwall cooling hole patterns were placed. All film-cooling holes injected at a 30 deg angle with respect to the endwall surface. The primary difference

Table 1 Summary of Cooling Hole and Slot Geometry

Feature	9× Scale
Re_{in}	2.3×10^5
Cooling hole diameter (cm)	0.46
Cooling Hole L/D	8.3
Hole injection angle	30 deg
P/D for leading edge holes	4/3
P/D for passage holes	3
Slot width (cm)	1.48
Slot length to width	1.8
Upstream slot location of vane	$-0.35C_a$
Slot injection angle	45 deg

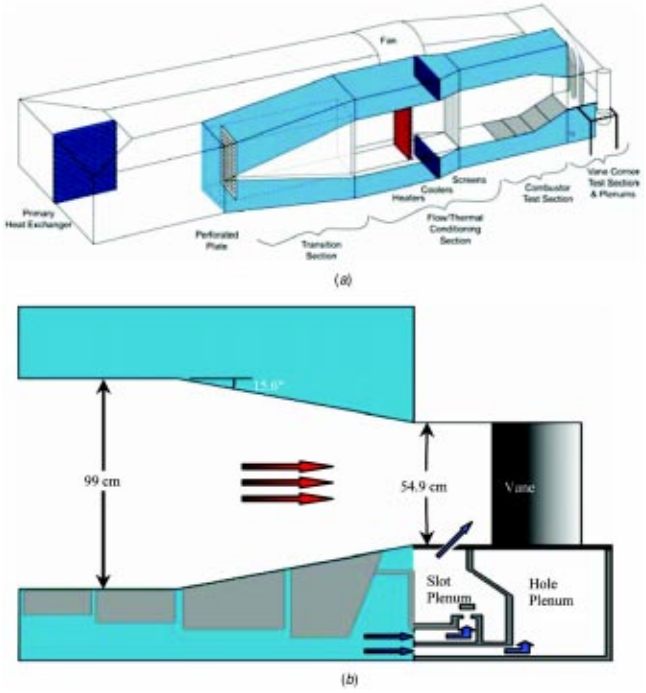

Fig. 2 (*a*) Illustration of wind tunnel facility, (*b*) cooling supply for slot and film cooling holes

between the two endwall cooling configurations in the leading-edge region was the absence of holes for pattern 2 where there would be a gutter between the two platforms. Inside the passage there are distinct differences between the two cooling hole patterns. Harasgama and Burton [18] suggested that locating film-cooling holes along iso-mach lines would ensure a uniform blowing rate and momentum flux helping to prevent jet liftoff. Hole pattern 1 was designed such that the cooling holes were located along straight lines approximating the iso-velocity contours. Iso-velocity contours were chosen because experiments will be conducted in a low-speed facility with little variation in Mach number. Alternatively, hole pattern 2 was designed such that the holes nearest to the pressure side of the vane lie on the same iso-velocity contours that were used in hole pattern 1, but with the difference being the row of holes was placed along axial lines rather than iso-velocity contours. There was a continuation of the gap left in the rows of holes where the previously mentioned gutterwould reside. While the hole pattern on the iso-velocity lines (pattern 1) provide a uniform blowing ratio given the same supply pressure, the axial hole pattern (pattern 2) is more likely to be cheaper to manufacture.

One of the additional differences between the two cooling hole patterns is that there were 14 more cooling holes for the cooling hole pattern 1 as compared with pattern 2, which was dictated by the designs given by industry (pattern 2 has 78% of the hole area of pattern 1). As a result of this disparity in the number of cooling holes, the coolant flow distribution is different for each of the hole patterns.

Experimental Methodology

Adiabatic endwall temperatures were measured for a range of experimental conditions using a scaled up vane, film-cooling holes, and slot geometries to allow for good measurement resolution. The experiments for this study were performed in a low-speed, closed-loop wind-tunnel facility, shown in Fig. 2(*a*), that has previously been described by Barringer et al. [19] and Colban et al. [11]. The flow in the wind tunnel is driven by a 50 hp axial vane fan, which is controlled by a variable frequency inverter.

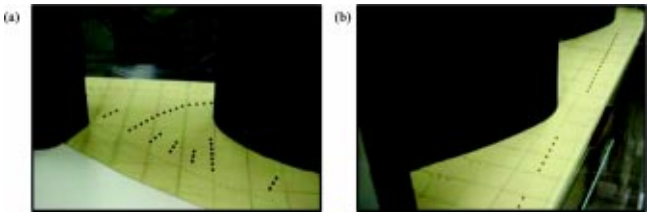

Fig. 3 Film-cooling holes for (*a*) Passage 1 and (*b*) the leading edge region

Downstream of the fan, the flow passes through a primary flow, finned-tube heat exchanger used to cool the bulk flow. After being turned by another 90 deg elbow, the flow encounters a three-way flow split. This flow split is controlled by a perforated plate, which was designed to obtain the proper pressure drop in the main gas path thereby forcing some of the air into the bypass legs. The core flow then passes through a heater bank, a series of screens used for flow straightening, and finally into a two-dimensional converging section. In the vane cascade, two full passages were modeled with three vanes. A bleed is positioned on either side of the two-passage cascade to remove edge effects from the side walls while tailboards ensure periodicity of the flow in the two passages.

As was stated, this facility included three channels: a heated primary channel (representing the main gas path) and two symmetric secondary channels (representing the coolant flow paths). A 35–40° C temperature differential between the coolant and mainstream was achieved by using the heaters in the primary channel and heat exchangers in the secondary channels. While the top secondary flow channel was closed off for these experiments, the bottom secondary flow channel was used for supplying the coolant to the slot and hole plenums, as seen in Fig. 2(*b*). These two plenums were constructed to provide independent control of the slot and film-cooling flow rates. The front plenum supplied the slot flow while the rear plenum supplied the film-cooling flow. Typical time to achieve steady-state conditions was 3 hr. As these experiments were to be relevant to industrial gas turbines where freestream turbulence levels can be lower than for aeroderivative engines; freestream turbulence effects were not the focus. The inlet turbulence level and length scales were measured, however, to be 1.3% and 4 cm, respectively.

The endwall test plate had a foam thickness of 1.9 cm (0.75 in.), which was chosen because of its low thermal conductivity (0.033 W/mK). To ensure the precision and integrity of the cooling hole pattern, the holes were cut with a five-axis water jet. Portions of the hole patterns are shown in Fig. 3. The endwall surface was painted black to enhance the radiative emissivity of the surface. The slot was constructed from balsa wood, which had the same thermal conductivity as the foam but was stiffer.

Coolant Flow Settings. For every test condition, the dimensionless pressure coefficient distribution was verified to ensure periodic flows were set through the passages (reported previously in [17]). Film-coolant flow rates for each cooling hole could not be controlled because only one plenum provided coolant to the entire endwall cooling hole pattern, and the local static pressure field varied greatly from hole to hole. Friedrichs et al. [1] suggested that a global blowing ratio based on the inlet flow conditions could be characterized by the blowing ratio of a loss-free hole injecting into inlet conditions as calculated from

$$M_{\text{ideal}} = \sqrt{\frac{\rho_c}{\rho_{in}} \cdot \frac{P_{o,c} - p_{s,in}}{P_{o,in} - p_{s,in}}} \tag{1}$$

A modification of this approach was taken for this study in that a global discharge coefficient C_D was derived so that the cumulative flow rate through either cooling pattern could be characterized. The C_D values were obtained from CFD studies and have been previously reported by Knost and Thole [16]. Measurements

Table 2 Discharge Coefficients for Film-Cooling

Slot flow rates $\%m_{\text{exit}}/M_{in}$	Film flow rate $\%m_{\text{exit}}/M_{in}$	Cooling hole patterns	Hole discharge coefficient
—	0.5/1.2	1	1.09
—	0.5/1.5	2	0.81
0.5/0.17	0.5/1.2	1	1.09
0.5/0.18	0.5/1.5	2	0.80
0.5/0.17	0.75/1.8	1	0.84
0.5/0.18	0.75/2.2	2	0.71

of the inlet velocity, average inlet static pressure, and coolant total pressures were obtained, which then allowed the fraction of coolant flow relative to the inlet core flow to be calculated from

$$\frac{\dot{m}_c}{\dot{m}_{\text{core}}} = M_{\text{ideal}} \cdot C_D \cdot \frac{A_{\text{hole}}}{A_{in}} \cdot \#\text{holes} \tag{2}$$

Different global discharge coefficients were used for each of the two cooling patterns, as indicated in Table 2, because the patterns had a number of holes in different locations. Note that these discharge coefficients are greater than one as a result of using a reference pressure as the static pressure at the inlet to the cascade. As the flow accelerates through the cascade the static pressure decreases, causing the discharge coefficient to be greater than one. A discharge coefficient of $C_D = 0.6$ was used for the slot flow. Also given in Table 2 is the global mass flux ratio (M_{in}) based on the inlet velocity. Note that for all of the experiments, the density ratio (jet-to-mainstream) was held fixed at 1.12.

Instrumentation and Measurement Uncertainty. An Inframetrics P20 infrared camera acquired the spatially resolved adiabatic temperatures on the endwall. Measurements were taken at 13 different viewing locations to ensure that the entire endwall surface was mapped. From a camera distance of 55 cm, each picture covered an area that was 24 cm by 18 cm with the area being divided into 320 by 240 pixel locations. The spatial integration for the camera was 0.715 mm (0.16 hole dia). The camera images were post calibrated using directly measured temperatures on the endwall by thermocouples that were installed. Thermocouple data was continuously acquired during image collection. The thermocouple measurements had a maximum-to-minimum range of approximately 0.8°C deg with a standard deviation of 0.17°C during the image collection time, which required about 30 min. For the post calibration, the emissivity and background temperature were adjusted until the temperatures from the infrared camera images were within 1°C of the corresponding thermocouple data. Typical emissivity values and typical background temperatures were $\varepsilon = 0.89$ and 45°C. Once the images were calibrated, the data was exported to an in-house Matlab® program that was written for image assembly.

Variations in free-stream temperature from passage to passage were less than 1.5°C. Three thermocouples were also located in both the slot and film-cooling plenums with one thermocouple beneath each of the passages and one beneath the center vane. These thermocouples allowed gradients in the coolant supply to be documented. Variation within the plenums was generally less than 0.3°C. Voltage outputs from the thermocouples were acquired by a 32-channel data acquisition module that was used with a 12-bit digitizing card.

An uncertainty analysis was performed on the measurements of adiabatic effectiveness using the partial derivative method described at length by Moffat [20]. The precision uncertainty was determined by taking the standard deviation of six measurement sets of IR camera images with each set consisting of five images. The precision uncertainty of the measurements was ±0.014°C. The bias uncertainty was ±1.0°C based on the calibration of the image. The bias uncertainty of the thermocouples was ±0.5°C. The total uncertainty was then calculated as ±1.0°C for the images and ±0.51°C for the thermocouples. The uncertainty in adiabatic effectiveness η was then found based on the partial derivative of η with respect to each temperature in the definition and the total uncertainty in the measurements. An uncertainty of $\partial\eta = \pm 0.082$ at $\eta = 0.2$ and $\partial\eta = \pm 0.029$ at $\eta = 0.9$ were calculated.

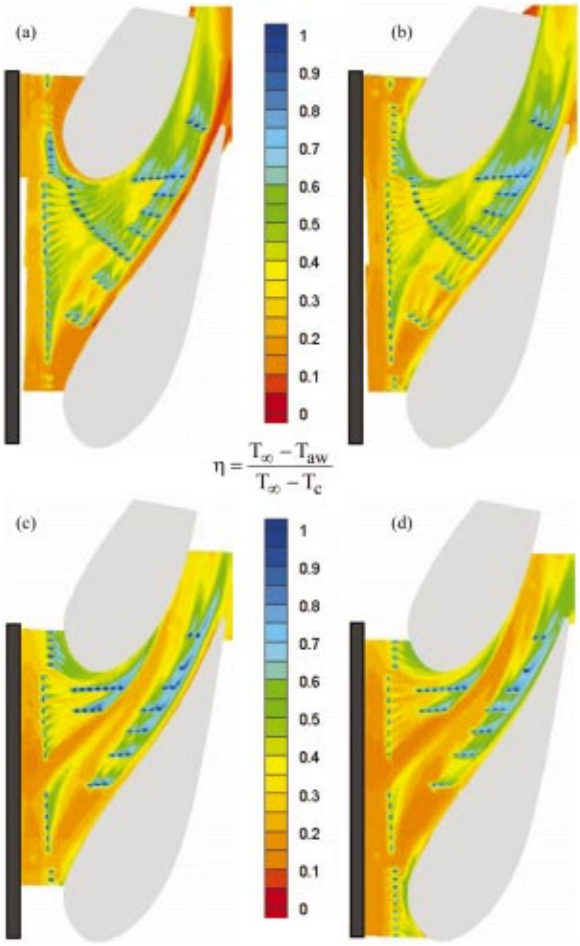

Fig. 4 Contours of adiabatic effectiveness for the baseline film-cooling only cases: (*a*) pattern 1, 0.5% coolant (*b*) pattern #1, 0.75% coolant, (*c*) pattern #2, 0.5% coolant, and (*d*) pattern 2, 0.75% coolant

Discussion of Results

The results from the experiments will be discussed in a logical progression of complexity. First, the cooling provided from the film cooling alone for both endwall patterns will be discussed. Second, the predictions for the combined slot and film-cooling configurations will be compared to the endwall film cooling alone. Finally, there will be a discussion of the leading-edge region and vane pressure-side region as these two regions were found difficult to cool.

Film Cooling Without Slot Injection. The film-cooling cases without slot flow for each of the two patterns are shown in Figs. 4(*a*)–4(*d*). The location of the slot, which was not simulated, is shown in black for reference. Each pattern was tested with a low and high film-cooling flow rate of 0.5% and 0.75% of the core flow, respectively. It can be seen in Figs. 4(*a*)–4(*d*) that the minimum effectiveness levels are $\eta = 0.1$ for all cases The reason for this is that there was a slight cooling effect of the near-wall fluid because of the long 4 m (6.8 *C*) unheated wall between the heater bank and the test section. The thermal boundary layer at the inlet to the cascade was measured to have a thick-

ness that was 5% of the vane span. As will be shown in later contours, effectiveness levels near zero were measured for some of the cases presented indicating the downturning of hotter fluid onto the endwall.

For pattern 1 at the low film flow rate, shown in Fig. 4(*a*), a fairly uniform coverage is seen across much of the passage. The leading row of holes near the suction side inject as discrete jets in the direction of the streamlines despite being directed normal to the inlet direction (toward the top of the page). The leading row of holes near the pressure side inject in a more merged pattern toward the injection direction. Just upstream of the stagnation location are quite ineffective at these low-coolant flow conditions, particularly near the pressure side. Those holes near the stagnation location along the suction side are swept around the shoulder leaving an uncooled region at the vane-endwall junction. The jets along the pressure side appear to inject in the streamwise direction following the contour of the vane despite the jet hole being directed axially downstream. Along the pressure side of the vane, however, there is still a warm region with no appearance of coolant.

For the increased film-cooling case of pattern 1, shown in Fig. 4(*b*), several effects are seen. First the suction-side jets of the leading row still inject as discrete jets, but lower adiabatic effectiveness values present downstream of the holes indicate that the jets are lifting off of the surface. The leading row of holes near the pressure side appear to be slightly more directed with very little coolant present downstream of several of the holes. The leading-edge holes at the stagnation location of pattern 1 for the 0.75% coolant flow rate are far more effective than for the 0.5% coolant flow rate. These higher effectiveness levels at the higher coolant flow are even more apparent along the suction side at cooling the vane-endwall junction. The cooling jets exiting the stagnation holes on the pressure side, however, appear to lift off at the injection location, impact the vane, and convect down the vane onto the endwall. This liftoff is evidenced by the coolant accumulating along the vane-endwall junction near the dynamic stagnation point of the vane. Within the passage, the pressure-side jets penetrate to approximately one cooling-hole diameter closer to the vane as compared with the 0.5% case, thereby reducing, but not eliminating, the warm zone along the pressure side.

For pattern 2 at the low blowing rate, shown in Figure 4(*c*), the most noticeable feature is the large hot streak through the center of the passage. This hot streak exists in the location where the gutter would be, therefore, including the gutter flow may tend to alleviate the problem. It is also important to remember that pattern 2 has fewer cooling holes, and as such, the coolant distribution is different from pattern 1. Consider the leading-edge row of holes where the holes nearer to the suction side inject with the streamlines for both hole patterns, but the local effectiveness levels are lower for pattern 2 than in the corresponding case for pattern 1. The reason for this difference is that pattern 2 has slightly higher momentum flux ratios for these jets, and as such, there is a tendency for the coolant flow to separate from the wall. These higher momentum flux ratios for pattern 2 has a positive benefit, however, when considering the holes near the stagnation location where the effectiveness levels are much higher for pattern 2 than for pattern 1 at the 0.5% coolant flow. Also, the pressure-side holes in the passage of pattern 2 appear to reduce the uncooled zone along the vane-endwall junction when compared to pattern 1.

The results of increasing the film-cooling flow rate, in pattern 2, to the high-blowing rate are shown in Figure 4(*d*). The jet detachment of the suction-side leading row of holes appears to be exacerbated, resulting in low effectiveness levels on the endwall. The coolant from the suction-side leading row of holes also appears to be less effective at the high-coolant flow rate and may suffer from blockage by the holes directionally downstream (bottom to top on the image) in the row causing the coolant to lift off. At the stagnation location, there is clearly a separation region of the jets that then impact the vane and wash onto the endwall surface. Within the passage, the pressure-side jets appear well merged and penetrate to the vane-endwall junction, eliminating the hot zone along the second half of the pressure side.

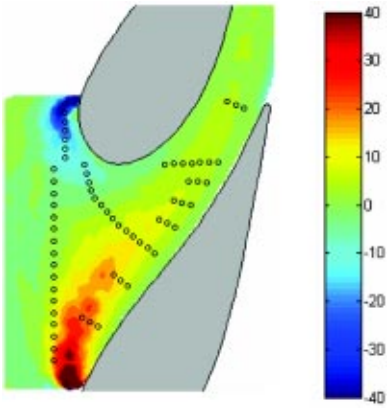

Fig. 5 Contours of the difference between the predicted flow angles at 2% span and midspan are shown for the high 0.75% slot flow case. The hole locations of pattern 1 are shown for reference.

Slot-Flow Combined With Film-Cooling Injection. When placing film-cooling holes, a designer would like to predict the film-coolant trajectory to ensure that the cooling needs of critical areas are met. A first approximation might be made by using a 2D inviscid CFD prediction of the streamlines to predict the path of the coolant. This first approximation was examined by comparing the flow-turning angles at the midspan relative to those near the endwall at the 2% span location. Contour plots of the difference between the flow-turning angles near the wall and those at midspan for a 0.75% slot-flow injection is shown in Fig. 5 (note that there is no film-cooling injection, but the cooling holes for pattern 1 are superimposed for reference). These predictions were computed using FLUENT, whereby the full details are given in a previous publication [16]. These contours indicate the cross flows that are induced in the near wall region for a high slot flow with deviations from the midspan by as much as 40 deg near the stagnation location. As will be discussed when interpreting the film-cooling measurements, it is relatively important to assess these differences when designing an endwall hole pattern.

To compare the influence of the slot flow rate, the 2% span streamlines for both the 0.5% and 1% slot flow cases were superimposed on hole pattern 1 as shown in Fig. 6. It is seen that especially along the upstream portion of the pressure side, and the upstream portion along the suction side to a lesser extent, the near-wall flow trajectory can be dramatically altered depending on the slot flow rate. At a high slot flow rate, the streamlines are drawn toward the suction side of the vane more so than at the lower slot flow rate. The cross flows are also shown to be slightly stronger at the high slot flow rate.

Predicted streamlines in the near-wall region (2% span) for 0.5% slot flow without film cooling are shown superimposed on adiabatic effectiveness measurements of the two patterns with 0.5% slot flow and 0.5% film flow in Figs. 7(*a*) and 7(*b*). For both hole patterns, the slot flow is funneled toward the suction side and is not present in the stagnation region. Similar to that of the film-cooling injection without slot flow, the minimum effectiveness level is $\eta = 0.1$, which is due to the unheated entry region to the cascade. It is apparent from these contours that the holes at the stagnation location, similar to those results in Fig. 4(*a*), are quite ineffective, leaving an uncooled area in the stagnation region. Moreover, it is apparent that the leading row of holes placed in the midpassage is being saturated by coolant and the need for film-cooling holes has been diminished as a result of the coolant from the slot.

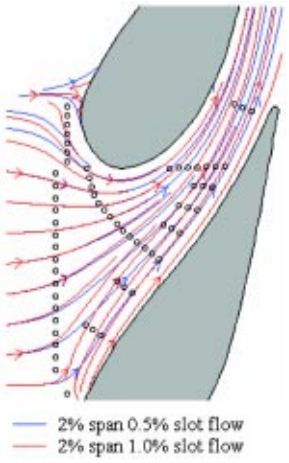

Fig. 6 Predicted streamlines at 2% span for both the 0.5% and 1.0% slot flow rates. The hole locations of pattern 1 are shown for reference.

For both patterns the film-coolant trajectories follow the predicted streamlines quite well in a number of locations. The coolant from the holes in the stagnation region is swept around the suction side and the jets along the pressure side of the vane follow the predictions. The largest difference between the streamlines and the coolant trajectory is for the leading row of holes nearer to the pressure side of the vane outside of the influence of the slot. This location shows that the holes are directed in a cross-pitch direction rather than following the streamlines at this location. It is also seen that the streamlines are more closely followed for pattern 1 relative to pattern 2, which can be explained by the stronger effects that the jets have for pattern 2 (fewer holes with more mass flow per hole).

Predictions of the streamlines at 2% span for the highest 1% slot flow rate are superimposed on measurements of each pattern with 0.75% slot coolant and 0.5% film-cooling in Figs. 8(*a*) and 8(*b*). The case of 0.75% slot coolant without film-cooling was not computed, but the predicted streamlines for the higher slot flow case will still be used to illustrate the effects of the slot flow.

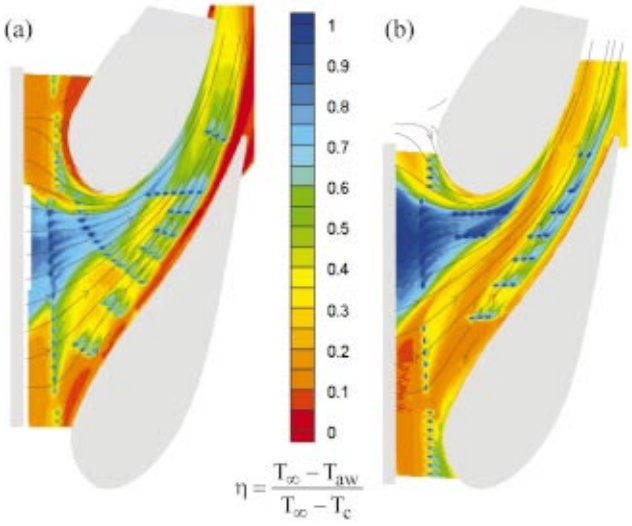

Fig. 7 Predicted streamlines at 2% span for 0.5% slot flow without film cooling are superimposed on measured effectiveness levels for (*a*) pattern 1 with 0.5% slot flow and 0.5% film cooling and (*b*) pattern 2 with 0.5% slot flow and 0.5% film cooling

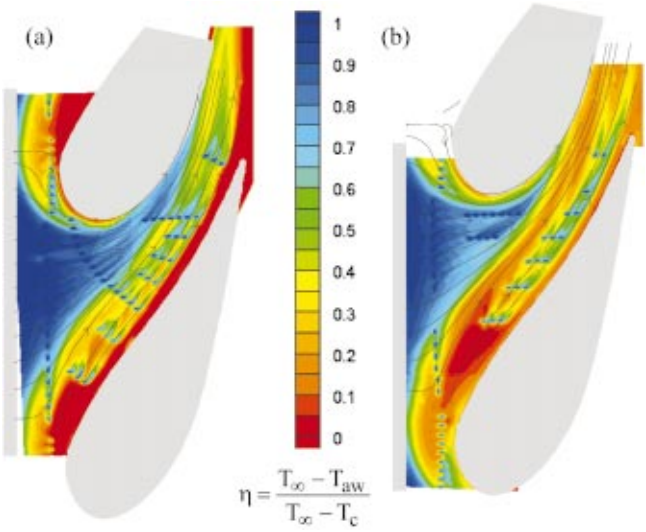

Fig. 8 Predicted streamlines at 2% span for 1% slot without film cooling superimposed for (*a*) pattern 1 with 0.75% slot flow and 0.5% film cooling, and (*b*) pattern 2 with 0.75% slot flow and 0.5% film cooling

When the slot flow is increased to 0.75% of the core flow while the film cooling is maintained at 0.5%, it is seen from Figs. 8(*a*) and 8(*b*) that the slot coolant coverage is dramatically increased. Coolant exits across the entire width of the slot, but is still funneled toward the suction side. Adiabatic effectiveness levels across much of the upstream portion of the endwall are near unity, indicating overcooling by the slot. The leading row of holes over a large portion of the pitch appears to be unnecessary for endwall cooling. Therefore, the coolant emerging from these holes could be redistributed to more advantageous locations. As has consistently been the case, the stagnation holes of pattern 1 at the low film-cooling rate are ineffective leaving an uncooled zone at the leading edge as the coolant is immediately swept around the suction side. Also, the pressure-side jets in the passage inject with the streamlines, once again leaving an uncooled region along the pressure side.

For these high slot flow conditions shown in Figs. 8(*a*) and 8(*b*), it is interesting to note that the minimum effectiveness level is $\eta = 0$ as compared to the previously shown no and low slot flow cases. The reason for these lower effectiveness levels is because of the increased downturning of the fluid above the endwall toward the endwall. These results indicate that for the high slot flow case there is a more pronounced cross-passage flow whereby the slot flow moves endwall fluid toward the suction side of the airfoil. As such, the near-wall upstream boundary layer fluid is replaced with hotter fluid that was entrained toward the endwall from above the 5% vane span location (thickness of the cooled thermal boundary layer).

The near-wall streamlines again predict the coolant trajectories relatively well. The leading row of holes follows the streamlines as do the pressure-side holes both in the up- and downstream regions. Note that there is better agreement with the streamlines for the leading row of holes in the region nearer to the pressure side of the vane for this high-coolant flow condition as compared with lower coolant flow.

When comparing the two hole patterns for combined film-cooling and slot flow cases, there are some noticeable differences. The exit location of the slot flow is seen to have migrated slightly toward the suction side of the vane for pattern 2 relative to pattern 1. This is most likely because of the absence of holes (due to the gutter location) for pattern 2, thus resulting in less flow blockage of the slot flow as compared to pattern 1 with a continual row of holes. Also immediately noticeable is the large hot streak through

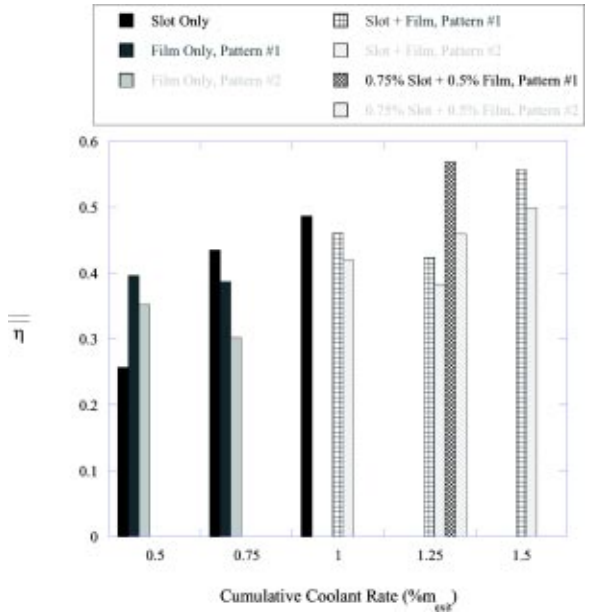

Fig. 9 Area-averaged effectiveness levels for a range of coolant flow rates (percentage is based on total passage flow)

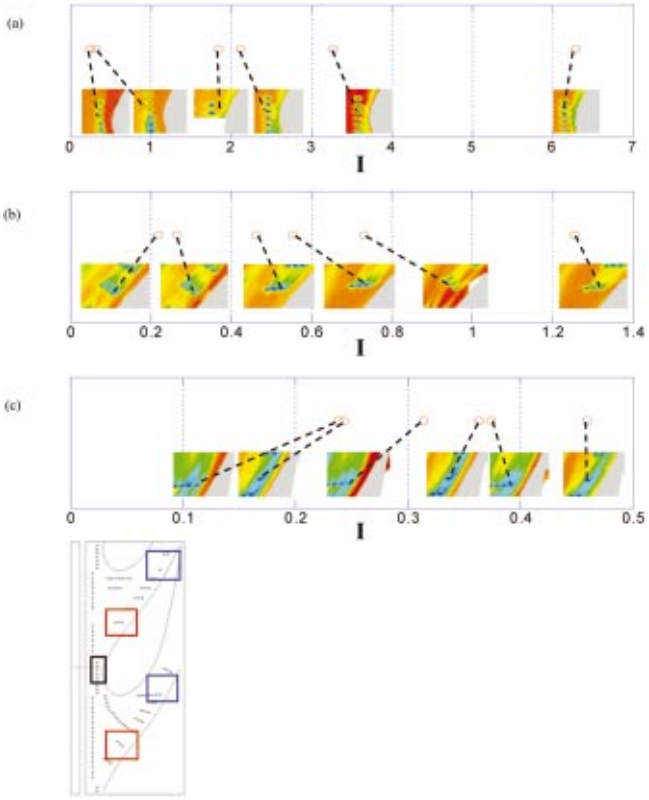

Fig. 10 Momentum flux ratios for holes indicated by the dashed lines are shown in (*a*) leading edge, (*b*) pressure side upstream, and (*c*) pressure side downstream regions. Hole locations are shown to the right

the center of the passage that was present without slot flow for pattern 2. The coolant from the pressure-side leading row of holes, which provided a small measure of relief to the hot streak without the presence of slot flow, appears drawn across the gap and merges with the slot coolant at the upstream rows of passage holes. One more noticeable difference between the two patterns is that the pressure-side jets in the passage of pattern 2 at the low blowing ratio are seen to be more directed than their counterparts in pattern 1 because of the higher momentum due to fewer jets. The coolant, however, still fails to fully penetrate to the vane, leaving a thin uncooled zone along the pressure side for both hole patterns.

Area-averaged adiabatic effectiveness levels, such as those shown in Fig. 9, are one way of deducing an overall comparison of the different cooling methods. This comparison, however, does not allow one to compare hot spots that may arise causing reductions in component life. The averages, shown in Fig. 9, were computed from the axial location $x/C_a=-0.24$, corresponding to the location furthest upstream where the images covered the entire pitch for all cases, to $x/C_a=0.74$, beyond which there was no optical access. The various cases, of which not all have been shown in this paper, have been grouped by cumulative coolant flow rate to provide a quantification of the effects of distributing coolant between the slot and film-cooling holes.

It is seen that at the lowest coolant flow rate of 0.5%, the film-cooling holes provide a greater average cooling effectiveness than the slot flow alone. When the coolant and slot flow rates are increased to 0.75% of the core flow, however, the slot flow provides the highest average effectiveness level. Note that the slot average effectiveness is only high in the upstream, center portion of the passage, while providing no relief to the vane-endwall junction along both the leading edge and pressure side of the vane. The average effectiveness level of pattern 1 is roughly the same for both coolant flows cases (0.5% and 0.75%), while pattern 2 actually performs worse at the higher coolant flow relative to the lower coolant flow. This worse performance is because of the jet separation and a widening of the hot streak in the center of the passage (these contours are not shown in this paper). At 1% coolant flow, the area averaged effectiveness level is still somewhat higher for the slot flow alone relative to the combined film and slot cases.

The 1.25% grouping consisted of four cases where the coolant was varied between slot and film-cooling holes as shown in Fig. 9. The highest average effectiveness level was measured for pattern 1 at the higher slot flow combined with lower film-cooling flow. Pattern 2 showed the same trend with the high-slot, low-film condition flows outperforming the low-slot, high-film flow case. The higher slot flow rate provided significantly more coolant to the broad uncooled area in the upstream portion of the passage. This, combined with the less directed, streamwise injection of the pressure-side holes, minimized the hot streak for pattern 2.

Finally, the high 0.75% slot flow rate combined with the high film-cooling rate for each pattern is shown for the total 1.5% coolant flow cases in Fig. 9. Pattern 1 showed a slight decrease in average effectiveness levels from the high-slot, low-film case. The reason for these lower average effectiveness levels is because lower local effectiveness levels occurred as the jet liftoff became significant in many regions on the endwall. Pattern 2 exhibited a slightly higher average effectiveness level as the hot ring along the pressure surface was reduced in size.

Leading Edge and Pressure Side Holes. Because these results indicate that the leading-edge and pressure-side regions are so difficult to cool, a further analysis revealed the importance of the local jet momentum flux ratios. The holes within the boxes shown in Fig. 10 were selected as representative holes to analyze. The local momentum flux ratios for each of the holes were calculated from CFD predictions using

$$I=\frac{\rho_j v_j^2}{\rho_\infty v_\infty^2}=\frac{\rho_j(\dot{m}_j/\rho_j A_j)^2}{2(P_{o,c}-p_\infty)} \tag{3}$$

The momentum flux ratios for these holes are also plotted in Figs. $10(a)-10(c)$ along with subsets of the effectiveness contours for these representative holes.

Figure 10(a) shows the holes in the stagnation location. The blowing ratios for these holes are seen to be significantly higher than for holes along the pressure side despite the velocity of these jets being lower. This occurs because of the stagnating core flow. At the lowest momentum flux ratios, the coolant from the jets is seen to barely be present. In fact, the contours indicate that there is some coolant present upstream of the injection location and the presence of some coolant being swept around the suction side of the vane. The coolant occurring upstream of the holes is present as a result of the leading-edge horseshoe vortex sweeping the coolant upstream.

As the momentum flux ratio of the jets is increased to slightly above $I\sim 2$ in Fig. 10(a), coolant is swept on the vane endwall. As the momentum flux ratio is increased, the jet impacts the endwall then separates to impact the vane and wash down the vane onto the endwall. These contours for $I\sim 3.2$ show coolant is present on the endwall for this range of momentum flux ratios. At the highest momentum flux ratio case of $I\sim 6$, all holes are fully detached with effectiveness levels along the vane-endwall junction being higher than $I\sim 3.2$. This is because the coolant exits the holes, impacts vane, and is then washed down onto the endwall to provide a cooling benefit.

The momentum flux ratios for the pressure-side holes are important to understand to ensure no uncooled regions near the pressure side of the vane. For the upstream pressure-side holes, presented in Fig. 10(b), the jets appear fully attached up to $I=0.46$. At $I=0.55$ the effectiveness levels are not maintained as far downstream of the holes, indicating partial jet liftoff. Also, the upstream-most hole at $I=0.46$ is drawn away from the vane and toward the center of the passage. At the momentum flux ratio of $I=0.73$, the jet appears nearly fully detached. This data indicate that as the momentum flux of the jets is increased, the upstream pressure-side jets separate from the wall rather than penetrate to the pressure-side surface of the vane.

The downstream pressure-side jets, shown in Fig. 10(c), appear fully attached in all cases with a maximum momentum flux ratio of only $I=0.46$, being achieved because of the high mainstream velocities. As the momentum flux ratio was increased, the downstream pressure-side jets penetrated close to the vane finally impacting the vane at the highest momentum flux ratio of $I=0.46$.

When comparing all holes, separation was induced in the range $0.55\leqslant I\leqslant 0.73$. The upstream pressure-side holes separated before impacting the vane, while the downstream pressure-side holes were able to penetrate completely to the pressure side of the vane leaving no uncooled regions.

Conclusions

Measurements of endwall adiabatic effectiveness were presented for an extensive test matrix combining both coolant from a flush slot and film cooling from two distinct hole patterns. Film-cooling holes were shown to distribute coolant evenly throughout the passage, with the exception being a large uncooled streak down the center of the passage for the hole pattern that was designed as a provision of a gutter between two vane platforms. With slot and film-cooling flows present, there was a large region in the center of the inlet to the passage that was overcooled. This overcooling was particularly evident for the high (0.75%) slot flow case. For the case with high leakage losses, it seems that is would be beneficial to eliminate those film-cooling holes and use the coolant elsewhere, such as near the leading-edge or vane pressure-side regions. In general, the hole pattern that was derived from constant streamlines was better than the hole pattern that included axially placed holes and a gutter.

Predicted streamlines at 2% span with included slot flow were compared to those at the midspan with the former being superimposed on measurements of film-cooling effectiveness. A considerable deviation between the near-wall and midspan streamlines was observed and shown that the slot flow rate and near-wall effects must be considered when predicting film-coolant trajectory based on streamlines. The film-coolant trajectories as well as the slot-flow trajectory each affected the other. At high slot flows, the near-wall cross flows were increased, which, in turn, swept the jets closer toward the suction surface. At low slot flows, the first row of film-cooling holes provided blockage, allowing more uniform flow to exit the slot.

Film-cooling momentum flux ratios were shown to have a significant impact on cooling performance. The higher momentum flux associated with higher blowing allowed the coolant to penetrate to hard-to-cool areas at the leading edge and along the pressure side in the downstream region. Cooling jets at the leading edge had a tendency to separately impact the vane, and then wash onto the endwall. As the momentum flux ratio was increased for the jets along the pressure side in the upstream portion of the passage, there was a tendency for the jets to separate prior to being able to penetrate closer to the pressure-side surface. This is different from the phenomena for the downstream holes along the pressure-side surface where the jets had less tendency to separate and were able to penetrate to the pressure side of the vane, thereby reducing the warm ring around the vane.

Acknowledgments

This publication was prepared with the support of the US Department of Energy, Office of Fossil Energy, National Energy Technology Laboratory. However, any opinions, findings, conclusions, or recommendations expressed herein are those of the authors and do not necessarily reflect the views of the DOE. The authors thank David Candelori (Pratt & Whitney), Ron Bunker (General Electric), and John Weaver (Rolls-Royce) for their input on the endwall cooling hole patterns.

Nomenclature

C = true chord of stator vane
C_a = axial chord of stator vane
G = gutter in Fig. 1
I = momentum flux ratio
$\dot{m}$ = mass flowrate
M = mass flux ratio
P = vane pitch; hole pitch
P_o, p = total and static pressures
Re_{in} = Reynolds number defined as $\mathrm{Re}=CU_{in}/\nu$
s = distance along vane from flow stagnation
S = span of stator vane
T = temperature
x, y, z = local coordinates
u, v, w = local velocity components
U = velocity magnitude

Greek

η = adiabatic effectiveness, $\eta=(T_\infty-T_{aw})/(T_\infty-T_c)$
ρ = density
ν = kinematic viscosity

Subscripts

ave, - = pitchwise average at a given axial location
ave, = = area average of endwall, slot to trailing edge
aw = adiabatic wall
c = coolant conditions
inlet = inlet conditions
∞ = freestream conditions

References

[1] Friedrichs, S., Hodson, H. P., and Dawes, W. N., 1996, "Distribution of Film-Cooling Effectiveness on a Turbine Endwall Measured Using the Ammonia and Diazo Technique," ASME J. Turbomach., **118**, pp. 613–621.
[2] Friedrichs, S., Hodson, H. P., and Dawes, W. N., 1997, "Aerodynamic Aspects of Endwall Film-Cooling," ASME J. Turbomach., **119**, pp. 786–793.

[3] Friedrichs, S., Hodson, H. P., and Dawes, W. N., 1999, ''The Design of an Improved Endwall Film-Cooling Configuration,'' ASME J. Turbomach., **121**, pp. 772–780.
[4] Blair, M. F., 1974, ''An Experimental Study of Heat Transfer and Film Cooling on Large-Scale Turbine Endwalls,'' ASME J. Heat Transfer, **97**, pp. 524–529.
[5] Granser, D., and Schulenberg, T., 1990, ''Prediction and Measurement of Film Cooling Effectiveness for a First-Stage Turbine Vane Shroud,'' ASME Paper No. 90-GT-95.
[6] Roy, R. P., Squires, K. D., Gerendas, M., Song, S., Howe, W. J., and Ansari, A., ''Flow and Heat Transfer at the Hub Endwall of Inlet Vane Passages-Experiments and Simulations,'' ASME Paper No. 2000-GT-198.
[7] Burd, S. W., and Simon, T. W., 2000, ''Effects of Slot Bleed Injection over a Contoured Endwall on Nozzle Guide Vane Cooling Performance: Part I: Flow Field Measurements,'' ASME Paper No. 2000-GT-199.
[8] Burd, S. W., Satterness, C. J., and Simon, T. W., ''Effects of Slot Bleed Ijection over a Contoured Endwall on Nozzle Guide Vane Cooling Performance: Part II Thermal Measurements,'' ASME Paper No. 2000-GT-200.
[9] Oke, R., Simon, T., Burd, S. W., Vahlberg, R., ''Measurements in a Turbine Cascade Over a Contoured Endwall: Discrete Hole Injection of Bleed Flow,'' ASME Paper No. 2000-GT-214.
[10] Oke, R., Simon, T., Shih, T. Zhu, B., Lin, Y. L., and Chyu, M. ''Measurements Over a Film-Cooled, Contoured Endwall with Various Coolant Injection Rates,'' ASME Paper No. 2001-GT-140.
[11] Colban, W. F., Thole, K. A., and Zess, G., 2002, ''Combustor-Turbine Interface Studies: Part 1: Endwall Measurements,'' ASME J. Turbomach., **125**, pp. 193–202.
[12] Colban, W. F., Lethander, A. T., Thole, K. A., and Zess, G., 2002, ''Combustor-Turbine Interface Studies: Part 2: Flow and Thermal Field Measurements,'' ASME J. Turbomach., **125**, pp. 203–209.
[13] Zhang, L., and Moon, H. K., 2003, ''Turbine Nozzle Endwall Inlet Film Cooling–The Effect of a Back-Facing Step,'' ASME Paper No. GT-2003-38319.
[14] Kost, F., and Nicklas, M., 2001, ''Film-Cooled Turbine Endwall in a Transonic Flow Field: Part I–Aerodynamic Measurements,'' ASME Paper No. 2001-GT-0145.
[15] Nicklas, M., 2001, ''Film-Cooled Turbine Endwall in a Transonic Flow Field: Part II–Heat Transfer and Film-Cooling Effectiveness Measurements,'' ASME Paper No. 2001-GT-0146.
[16] Knost, D. K., and Thole, K. A., 2003, ''Computational Predictions of Endwall Film-Cooling for a First Stage Vane,'' ASME Paper No. GT-2003-38252.
[17] Radomsky, R. W., and Thole, K. A., 2000, ''Flowfield Measurements for a Highly Turbine Flow in a Stator Vane Passage,'' ASME J. Turbomach., **122**, pp. 255–262.
[18] Harasgama, S. P., and Burton, C. D., 1992, ''Film Cooling Research on the Endwall of a Turbine Nozzle Guide Vane in a Short Duration Annular Cascade: Part 1—Experimental Technique and Results,'' ASME J. Turbomach., **114**, pp. 734–540.
[19] Barringer, M. D., Richard, O. T., Walter, J. P., Stitzel, S. M., and Thole, K. A., 2002, ''Flow Field Simulations of a Gas Turbine Combustor,'' ASME J. Turbomach., **124**, pp. 508–516.
[20] Moffat, R. J., 1988, ''Describing the Uncertainties in Experimental Results,'' Exp. Therm. Fluid Sci., **1**, pp. 3–17.